

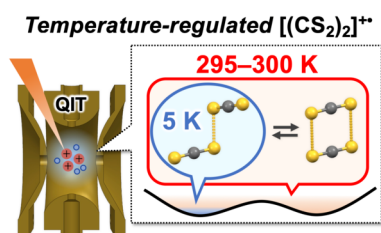
Correlation of Charge Resonance Interaction with Cluster Conformations Probed by Electronic Spectroscopy of Dimer Radical Cations of CO₂ and CS₂ in a Cryogenic Ion Trap

Masahiro Koyama, Satoru Muramatsu*, Yasuaki Hirokawa, Jidai Iriguchi, Akihito Matsuyama, Yoshiya Inokuchi*

Department of Chemistry, Graduate School of Advanced Science and Engineering, Hiroshima University, 1-3-1 Kagamiyama, Higashi-Hiroshima-shi, Hiroshima 739-8526, Japan

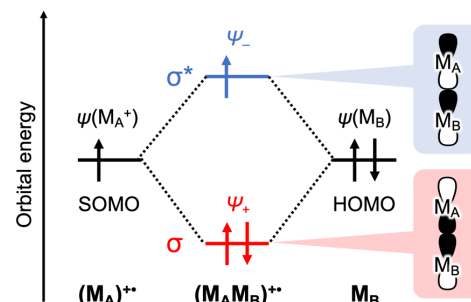
ABSTRACT: Radical cations of dimeric clusters of carbon dioxide/disulfide, [(CX₂)₂]⁺⁺ (X = O, S), form strong intracuster bonds through charge resonance (CR) interactions. We herein performed electronic photodissociation spectroscopy of [(CX₂)₂]⁺⁺ while regulating the temperature at ambient and cryogenic conditions using a quadrupole ion trap. Both ions exhibited broad band absorption in the near-infrared-visible light region; it is called “CR band”, a measure of the strength of the CR interaction. Strikingly, this band underwent a noticeable blueshift upon cryogenic cooling for [(CS₂)₂]⁺⁺, while not for [(CO₂)₂]⁺⁺. Based on quantum chemical calculations with a coupled cluster method, the band shift was attributed to the variations in the relative population of two energetically-close conformers found for [(CS₂)₂]⁺⁺. This study highlights a strong correlation between CR interactions and conformation of the radical dimer cations, demonstrating the exceptional significance of cryogenic cooling in the chemistry of ionic molecular clusters.

TOC Graphic:



Spectroscopic characterization of the electronic structures of molecular clusters is one of the most fundamental and intensively explored areas in cluster chemistry.^{1–5} The central focus of these investigations lies in understanding how intracuster (intermolecular) interactions are influenced by factors such as cluster size and constituent molecules. Of particular interest in this context is the charge resonance (CR) interaction, which is observed in a wide range of radical cations of molecular dimers. These ions exhibit a unique two-center three-electron (2c-3e) bond, where electrons fully and singly occupy the σ and σ^* orbitals, respectively, formed by the overlap of HOMO orbitals of the constituent molecules (Scheme 1). In this bonding scheme, the total charge is distributed across the components. Since the formal bond order in this bonding mode is 0.5 (Scheme 1), such bonds are often referred to as semi-covalent bonds or hemibonds.^{6–13} Remarkably, the electronic transition from σ to σ^* orbitals in this bonding scheme, known as the CR transition, leads to a prominent absorption band in the near-infrared-visible region (CR band).^{14–}

Scheme 1. Schematic of Bonding and Anti-Bonding Orbitals of 2c-3e Bond.



¹⁸ Consequently, the spectroscopic characterizations have attracted considerable attention.^{16–19} Particularly, when the corresponding electronic ground and excited states (Ψ_{\pm}) are described as $\Psi_{\pm} = [\psi(M_A^+)\psi(M_B) \pm \psi(M_A)\psi(M_B^+)] / (2 \pm 2S)^{1/2}$, the CR transition energy (E_T) is directly related to the binding energy between the component molecules in the dimer ions (E_B), as illustrated in the following relationship (eq. 1):¹⁸

$$E_T = \frac{2E_B}{1 - S} \quad (1)$$

Here, S represents the overlap integral between the constituent molecules.

One of the gold standards for producing molecular cluster ions is by combining the generation of neutral clusters through supersonic expansion with the ionization by crossed electron beams, a method pioneered by Märk, Lineberger, and others.^{14,20,21} The ionization step of this technique includes cluster heating via electron impact and subsequent cooling via evaporation of excess molecules, which are balanced to eventually achieve a typical

average internal temperature of ~ 100 K for the cluster ions.^{22–24} Owing to the relatively weak intracluster interactions compared to the typical intramolecular chemical bonds, the clusters at this temperature range frequently exhibit high fluxionality—facile isomerization between energetically close conformers.^{25–28} Since the intracluster interactions are generally strongly correlated with the cluster conformations,^{26,27,29,30} regulation of the internal temperature of the clusters, particularly under cryogenic conditions, remains a significantly challenging aspect that has not been adequately addressed in the extensive research conducted over the decades. Indeed, a recent spectroscopic study utilizing superfluid helium nanodroplets at sub-Kelvin temperatures successfully identified the hemibonded isomer of $[(\text{H}_2\text{O})_2]^+$ formed through CR interactions.⁸ This is a notable achievement, as conventional methods typically yield the proton-transferred isomer $[\text{H}_3\text{O}^+-\text{OH}]$.³¹ Thus, the study highlights the significance of cryogenic cooling for structural investigations of molecular cluster ions.

In this study, we focused on the regulation of cluster ion temperatures through the implementation of a cryogenic ion trap, where the typical vibrational temperature of the stored ions has been estimated to be ~ 10 K.³² This technique has been recently utilized typically together with an electrospray ionization method for the structural analyses of a wide range of gaseous molecular ions.^{33–42} By combining the cryogenic ion trap with above-described cluster ion source, the steps of the ion formation and the thermalization are separated and precise temperature regulation of molecular cluster ions, particularly under cryogenic conditions, will be achieved. In this sense, we expect this study would broaden the capability of this cryogenic ion trap-based spectroscopic techniques. Specifically, we herein focused on the radical cations of carbon dioxide and carbon disulfide dimers $[(\text{CX}_2)_2]^+$ ($\text{X} = \text{O}, \text{S}$) as target clusters. They have been extensively examined for decades as prototypical examples of ions exhibiting the CR interaction.^{9,10,14,15,20,43–51} The dimer ions serve as highly stable ion cores in larger clusters, $[(\text{CX}_2)_n]^+$ ($n \geq 3$), as revealed by infrared photodissociation (IR-PD) spectroscopy.^{44,47} Regarding electronic spectroscopy, the broad CR band of $[(\text{CO}_2)_2]^+$ at $12500\text{--}25000\text{ cm}^{-1}$ has been reported under ambient temperature conditions.^{14,15} This study aims to investigate how the CR interaction in $[(\text{CX}_2)_2]^+$ appear under temperature-regulated conditions using near-infrared-visible photodissociation (NIR-Vis-PD) spectroscopy. We will establish how the band profile evolves with temperature change and discuss the correlation with the cluster conformations as well as the CR interactions.

Figure 1 shows the schematic diagram of the photodissociation spectrometer that has been developed in this study. The spectrometer comprises a cluster ion source, an octupole ion guide (OPIG), a quadrupole ion trap (QIT), and a time-of-flight mass spectrometer (TOF-MS); details are provided in Supporting Information.^{32,44,47,52–55} Briefly, target clusters, $[(\text{CX}_2)_2]^+$ ($\text{X} = \text{O}, \text{S}$), were generated by crossing neutral CO_2 or CS_2 clusters in a supersonic free jet with an electron beam. The generated ions were guided by the OPIG and introduced into the QIT (Figure S1) operating at ambient (295–300 K) or cryogenic (5 K) temperature. The thermalized $[(\text{CX}_2)_2]^+$ ions, via collisions with He buffer gas in the QIT, were irradiated with a near-infrared-visible laser light ($10000\text{--}24000\text{ cm}^{-1}$; $1000\text{--}420\text{ nm}$) using an optical parametric oscillator. The resulting photofragment ions and the remaining target ions were detected using the TOF-MS. The mass spectra obtained with and without photoirradiation at 16130 cm^{-1} (620 nm) are shown in Figure S2. Depletion and appearance of the mass peaks of $[(\text{CX}_2)_2]^+$ and $(\text{CX}_2)^+$, respectively, indicated the photodissociation process described in reaction (2). The linearity against laser fluence was confirmed, as shown in Figure S3.



Figure 2 shows the NIR-Vis-PD spectra of $[(\text{CX}_2)_2]^+$ recorded by monitoring the fragment ion $(\text{CX}_2)^+$ as a function of the laser wavenumber. At ambient QIT temperature (295–300 K), a broad absorption band over the entire measurement region ($10000\text{--}24000\text{ cm}^{-1}$) was observed for $[(\text{CO}_2)_2]^+$. This band was almost identical to that observed in a previous study in which the ions were thermalized at room temperature in a drift tube,¹⁵ and the observed band was identified as the CR band.⁴⁹ Similarly, at ambient temperature, $[(\text{CS}_2)_2]^+$ exhibited a broad absorption band with an apparent maximum at $12000\text{--}14000\text{ cm}^{-1}$, which was identified as the CR band. The overlap integral S in eq. 1 is often considered negligible for simple estimation of the CR interaction. Accordingly, the roughly estimated binding energy of $[(\text{CO}_2)_2]^+$ and $[(\text{CS}_2)_2]^+$ was $\sim 7000\text{ cm}^{-1}$, which is significantly larger than that of heterodimeric radical cations such as $[\text{CO}_2\text{--X}]^+$ ($\text{X} = \text{H}_2\text{O}, \text{CH}_3\text{OH}$).^{7,57} This result reflects the degree of charge delocalization in the dimer cations—a smaller difference between the ionization potentials of two molecular components cause efficient charge delocalization and thus larger CR interactions.¹²

Whereas the NIR-Vis-PD spectra of $[(\text{CO}_2)_2]^+$ and $[(\text{CS}_2)_2]^+$ at ambient temperature were similar, their behavior at a reduced QIT temperature of 5 K was totally different. In the case of

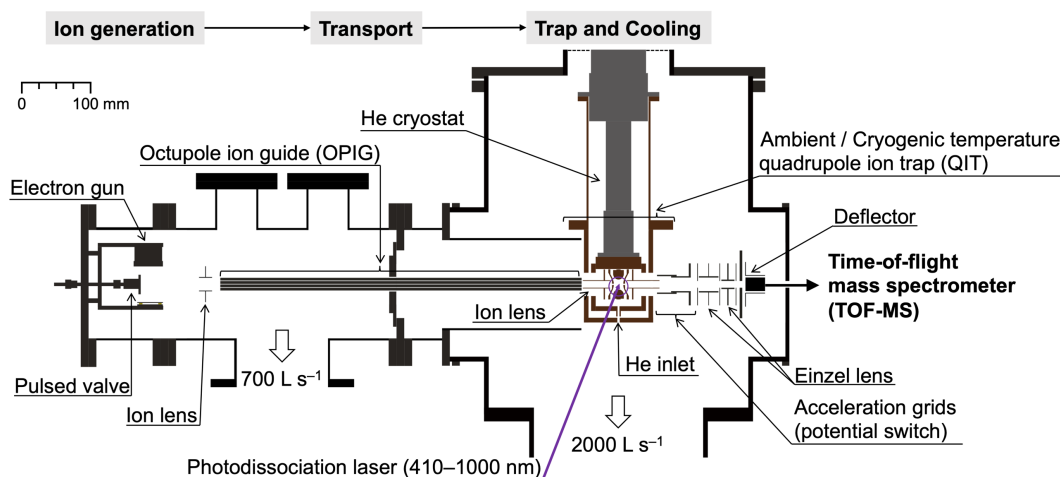


Figure 1. Schematic diagram of the photodissociation spectrometer developed in this study.

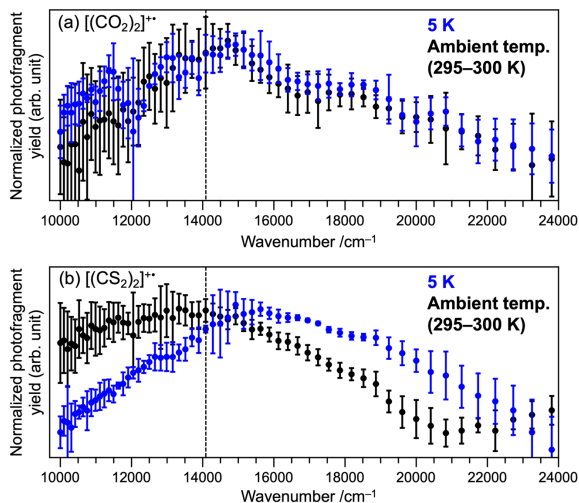


Figure 2. NIR-Vis-PD spectra of (a) $[(\text{CO}_2)_2]^{2+}$ and (b) $[(\text{CS}_2)_2]^{2+}$. The blue and black spectra were recorded at QIT temperatures of 5 K and ambient temperature (295–300 K), respectively. The spectra in regions $<14085 \text{ cm}^{-1}$ and $>14085 \text{ cm}^{-1}$ (710 nm) were recorded and plotted separately, because of the switching of the oscillation modes. The intensities are normalized at the band maximum (more details in Supporting Information).

$[(\text{CO}_2)_2]^{2+}$, the CR band position was almost identical to that at ambient temperature (Figure 2a). Here, it should be noted that the broad profile was observed even under cryogenic conditions. This indicates that the bandwidths are intrinsically determined by the shape of the potential surface of the electronic excited state, rather than by the contribution from thermal effects. This is consistent with previous studies that have assumed a repulsive character of the potential surfaces for the excited states formed by CR transitions.^{46,51} In contrast to $[(\text{CO}_2)_2]^{2+}$, $[(\text{CS}_2)_2]^{2+}$ exhibited a maximum at 15000–17000 cm^{-1} at QIT temperature of 5 K (Figure 2b), which was blueshifted relative to the band at ambient temperature (295–300 K). Based on eq. 1, this blueshift apparently indicates that the strength of the CR interaction in $[(\text{CS}_2)_2]^{2+}$ is sharply dependent on temperature, whereas that in $[(\text{CO}_2)_2]^{2+}$ was independent of the temperature.

To understand the cause of the temperature-dependent band shift of $[(\text{CS}_2)_2]^{2+}$, we performed quantum chemical calculations using a coupled cluster method with the cluster operators of single and double excitations (CCSD) with basis sets of aug-cc-pVTZ (more details in Supporting Information; Table S1 presents a comparison with the DFT-calculated results).⁵⁶ Extensive survey of the optimized structures at our computational level yielded a single isomer of $[(\text{CO}_2)_2]^{2+}$ (conformer **S**; Figure 3a) with a C_{2h} symmetry and COOC dihedral angle of 180.0° . This corresponds to the commonly called “staggered” form and is consistent with previous theoretical studies.^{20,45–51} The O–O bond length, which was calculated to be 2.09 Å, was shorter than the sum of the van der Waals radii of O atoms (3.04 Å)⁵⁸ and longer than the typical O–O single bond (1.48 Å).⁵⁸ This qualitatively corresponds to a formal bond order of 0.5 in the 2c-3e bonding mode (Scheme 1). In contrast, two isomers were revealed for $[(\text{CS}_2)_2]^{2+}$ (Figure 3a). One of the isomers had a S–S bond distance of 2.69 Å and CSSC dihedral angle of 102.1° (conformer **S'**; C_2), which was close to the dihedral angle in the staggered form. In the other isomer, two CS_2 units faced each other, with a CSSC dihedral angle of 0.0° (conformer **F'**; D_{2h}). In this conformer, two S–S bonds were formed, but each bond (3.13 Å) is longer than that of conformer **S'**

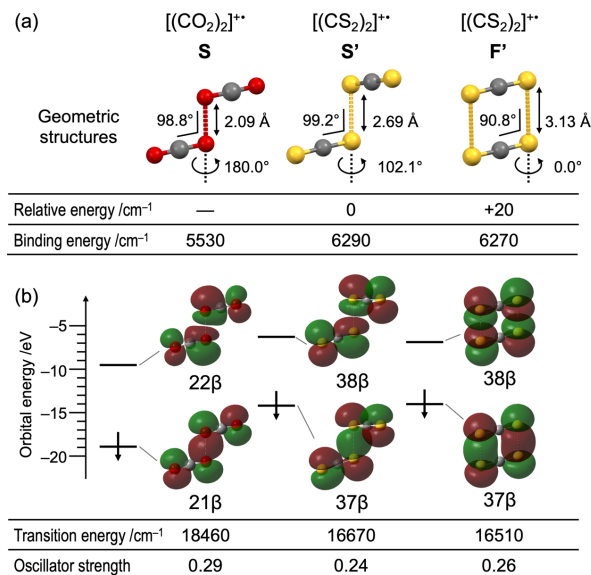


Figure 3. (a) Geometric structures of $[(\text{CX}_2)_2]^{2+}$ ($\text{X} = \text{O}, \text{S}$) optimized at the CCSD/aug-cc-pVTZ level. The XX bond lengths, the CXX angles, and the CXXC dihedral angles are indicated. Relative energy without vibrational zero-point corrections for $[(\text{CS}_2)_2]^{2+}$ (with respect to conformer **S'**) and binding energy (with respect to $\text{CX}_2 + (\text{CX}_2)^{2+}$) are shown in tabular form. (b) Orbital energy and isodensity surface of molecular orbitals of $[(\text{CX}_2)_2]^{2+}$ ($\text{X} = \text{O}, \text{S}$) that contribute to $\text{D}_3 \leftarrow \text{D}_0$ transitions. Transition energy and oscillator strength are shown in tabular form.

(2.69 Å); this results in almost comparable total energy (higher stability of conformer **S'** only by 20 cm^{-1} at our computational level). It should be noted that the previous theoretical studies on $[(\text{CS}_2)_2]^{2+}$ ^{43,44} did not consider conformer **F'** as it could not be obtained using the DFT calculations at the B3LYP/6-311+G(d) level. Figure 3b summarizes the electronic excitation energies, oscillator strengths, and related molecular orbitals of the $\text{D}_3 \leftarrow \text{D}_0$ transitions of these isomers calculated using the equation-of-motion (EOM)-CCSD method. The bands in the NIR-Vis-PD spectra (Figure 2) corresponded to these transitions, since the excitation energies of the other transitions were very different from the measurement window in this study (Table S2). Regardless of the isomers, the calculated $\text{D}_3 \leftarrow \text{D}_0$ excitations can be regarded as the transition from a bonding to an anti-bonding orbital of the 2c-3e bond, consistent with the assignment as CR bands. Regarding $[(\text{CS}_2)_2]^{2+}$, the conformer **S'** has 160 cm^{-1} larger excitation energy (16670 cm^{-1}) than the conformer **F'** (16510 cm^{-1}).

The structural difference between $[(\text{CO}_2)_2]^{2+}$ and $[(\text{CS}_2)_2]^{2+}$ is associated with the two-dimensional relaxed potential energy surfaces (PESs) of the electronic ground (D_0) states (Figure 4), where the X–X bond distances (R) and the CXXC dihedral angles (Φ) were selected as the representative geometrical parameters. Note that the PESs were calculated by using the double-zeta basis sets (CCSD/aug-cc-pVDZ) due to the computational costs; we found that the order of relative stability and excitation energy between conformers **S'** and **F'** are both inverted at this computational level (Figure S4), the overall discussions in this section remain valid. For $[(\text{CO}_2)_2]^{2+}$, only one potential minimum was obtained, corresponding to conformer **S** ($R = 2.1 \text{ Å}$, $\Phi = 180^\circ$). In contrast, two potential minima were found for $[(\text{CS}_2)_2]^{2+}$, corresponding to conformer **S'** ($R = 2.8 \text{ Å}$ and $\Phi = 100^\circ$) and conformer **F'** ($R = 3.3 \text{ Å}$ and $\Phi = 0^\circ$). This difference can be partly

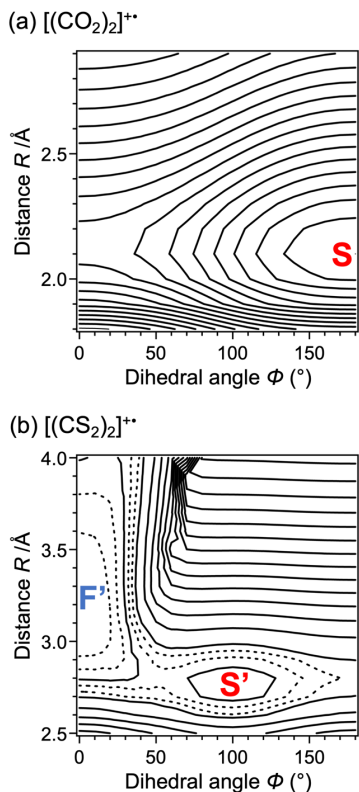


Figure 4. (a, b) Relaxed D_0 -state PESs of (a) $[(\text{CO}_2)_2]^+$ and (b) $[(\text{CS}_2)_2]^+$ calculated at the CCSD/aug-cc-pVDZ level without vibrational zero-point corrections. The XX bond distances (R) and the CXXC dihedral angles (Φ) were scanned by 0.1 \AA and 10° , respectively. The dotted and solid contours correspond to 100 and 300 cm^{-1} intervals, respectively.

described by the Φ -dependence of the σ and σ^* orbitals in the $2c$ - $3e$ bond (Scheme 1), as discussed in detail in Figure S5; the σ orbitals of $[(\text{CS}_2)_2]^+$ were sharply lowered at smaller Φ , possibly owing to the larger lobes that prevented steric repulsion between the C atoms of the two CS_2 moieties. The PES of the D_0 state indicates an isomerization barrier between the conformers of $[(\text{CS}_2)_2]^+$. The isomerization between S' and F' can be roughly considered as the rotation around the S–S bond associated with bond elongation, where the barrier was calculated to be as small as 350 cm^{-1} with respect to that of conformer F' at this computational level (further smaller barrier height of 150 cm^{-1} without zero-point corrections at full optimization at CCSD/aug-cc-pVTZ; Figure S6). On the other hand, the PESs of the photoexcited (D_3) states of $[(\text{CO}_2)_2]^+$ and $[(\text{CS}_2)_2]^+$ were similar, with both species exhibiting repulsive profiles along the R axis (Figure S7).

The correspondence between the temperature-dependent spectral changes in the NIR-Vis-PD spectrum (Figure 2b) and the presence of the conformational isomers (Figure 3) suggest that the band shift for $[(\text{CS}_2)_2]^+$ is attributable to the structural fluxionality, as schematically shown in Figure 5. At ambient temperature (295–300 K), conformers F' and S' are considered to coexist, based on the small relative energy and isomerization barrier. Assuming a Boltzmann distribution while using the relative energy of 20 cm^{-1} at the CCSD/aug-cc-pVTZ level, the relative population of conformers S' and F' is estimated to be 1:0.91 at 300 K.⁵⁹ If the less stable conformer has a smaller excitation energy, the significant contribution of the both conformers results in the apparently intense absorption at a smaller wavenumber region (12000 – 14000 cm^{-1}). In our current computational level at CCSD/aug-cc-pVTZ,

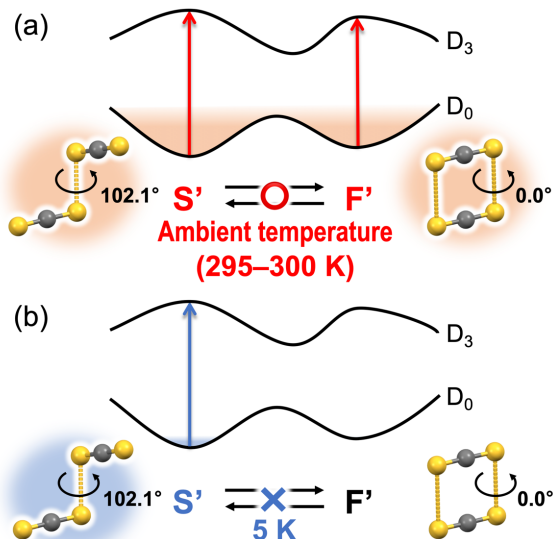


Figure 5. Schematic diagram of temperature-dependent structural fluxionality of $[(\text{CS}_2)_2]^+$. (a) At ambient temperature (295–300 K), conformers S' and F' coexist because of the small isomerization barrier. (b) At 5 K, the structure “freezes” at the most stable conformer S' , causing apparent blueshift in the NIR-Vis-PD spectra.

the conformer F' was calculated to be less stable and to have a smaller D_3 - D_0 transition energy (16510 cm^{-1}). It should be noted that quantitative analyses on the precise experimental excitation energy and/or abundance ratio of isomers from this spectrum are difficult, because of the largely broad profile of the CR bands and the possible contributions from the hot bands. In contrast, under cryogenic conditions (QIT temperature: 5 K, typical ion vibrational temperature: $\sim 10 \text{ K}$)³², only the more stable conformer is expected to be predominant; the estimated relative S' : F' population by assuming the same relative energy (20 cm^{-1}) at 10 K is 1:0.07. The more stable conformer S' was calculated to have a higher excitation energy (16670 cm^{-1}). Accordingly, the absorption band appeared in the higher wavenumber region. This result is partly consistent with the previous IR spectroscopy study of $[(\text{CS}_2)_2]^+$ in cold Ar and Ne matrices; the study concluded the presence of a single conformer with a single anti-symmetric S–C–S stretching vibration peak at 1360 – 1400 cm^{-1} .⁴³ Note that the structure of this conformer was considered to be that with $\Phi = 180^\circ$, rather than conformer F' ($\Phi = 0^\circ$) or S' ($\Phi = 100^\circ$). This discrepancy seems to be owing to the difference in computational levels. At the CCSD level in our current investigation, the conformer with $\Phi = 180^\circ$, which was predicted to be a local minimum structure at DFT calculations (B3LYP functional), was rather determined to be a transition state structure (Figure S6), while conformer S' instead may account for the observed IR band. For $[(\text{CO}_2)_2]^+$, on the other hand, the absence of such temperature-dependent band shift corresponds to theoretical prediction of the single conformer S , where the observed band is exclusively attributed to it regardless of temperature. The significant spectral change of $[(\text{CS}_2)_2]^+$ with isomer abundance demonstrates that the magnitude of the CR interaction is highly structure dependent. The apparently large band shift ($>1000 \text{ cm}^{-1}$) despite the small difference in the relative energy of the two conformers (20 cm^{-1} ; Figure 3a) suggests that the eq. 1 seems to be no longer good estimation for describing the correlation between the CR transition energy and the binding energy of the

component molecules. Consequently, this study may serve as a valuable benchmark for exploring better quantitative model for the CR-interacting systems. In this regard, however, the difference between the calculated electronic transition energy of the two isomers at the CCSD/aug-cc-pVTZ level (160 cm^{-1} ; Figure 3b) itself does not quantitatively agree with the apparent experimental band shift. One of the possible causes for this discrepancy can be a still inadequate computational level with regard to the quite shallow potential profiles. Particularly, the large dependence of the calculated relative and excitation energies of the conformers on the basis sets (Figure 3 and S4) implies the necessity for careful handling of these cluster ions computationally. Further detailed investigations of these factors for a comprehensive understanding of this cluster system will be conducted in our future studies.

In summary, we studied the correlation between the CR interaction in gas-phase radical cations of molecular dimers, $[(\text{CX}_2)_2]^+$ ($\text{X} = \text{O}, \text{S}$), and their geometric structures by NIR-Vis-PD spectroscopy at ambient and cryogenic temperatures. The absorption band of $[(\text{CS}_2)_2]^+$, attributed to CR transition, was apparently blueshifted upon cooling the ion trap from ambient temperature (295–300 K) to 5 K. In contrast, $[(\text{CO}_2)_2]^+$ did not exhibit such temperature-dependent band shift. CCSD calculations revealed two isomers of $[(\text{CS}_2)_2]^+$ characterized by the rotational angles around the S–S bond. The isomers had different CR transition energies, with a small energy barrier (in the order of $\sim 100\text{ cm}^{-1}$). In contrast, a single isomer was identified for $[(\text{CO}_2)_2]^+$. Based on these results, we concluded that the temperature-dependent band shift of $[(\text{CS}_2)_2]^+$ was caused by a change in the relative population of the two isomers. These results showed that the CR interaction energy is a sensitive reflection of the conformation of the radical cation of molecular dimers, demonstrating the exceptional ability of cryogenic ion-trap spectroscopy for molecular cluster ions that has a decades-long history of investigations. In other words, this study shed new light on unexplored frontiers at the interface of cluster chemistry and cryogenic science.

ASSOCIATED CONTENT SUPPORTING INFORMATION

The supporting Information is available free of charge at ***.

Experimental and theoretical methods, schematic details of the ion trap, functional dependence of DFT calculations, calculated $D_n \leftarrow D_0$ transition energies, Vis-PD mass spectra, laser power dependence of photodissociation, optimized structures at CCSD/aug-cc-pVDZ level, Walsh diagrams, transition state structures, 2D PESs of electronically excited state (D_3), full author list of refs 8 and 56.

AUTHOR INFORMATION

Corresponding Authors

Satoru Muramatsu – Department of Chemistry, Graduate School of Advanced Science and Engineering, Hiroshima University, Higashi-Hiroshima 739-8526, Japan; Email: smuramatsu@hiroshima-u.ac.jp

Yoshiya Inokuchi – Department of Chemistry, Graduate School of Advanced Science and Engineering, Hiroshima University, Higashi-Hiroshima 739-8526, Japan; Email: y-inokuchi@hiroshima-u.ac.jp

Authors

Masahiro Koyama – Department of Chemistry, Graduate School of Advanced Science and Engineering, Hiroshima University, Higashi-Hiroshima 739-8526, Japan

Yasuaki Hirokawa – Department of Chemistry, Graduate School of Advanced Science and Engineering, Hiroshima University, Higashi-Hiroshima 739-8526, Japan

Jidai Iriguchi – Department of Chemistry, Graduate School of Advanced Science and Engineering, Hiroshima University, Higashi-Hiroshima 739-8526, Japan

Akihito Matsuyama – Department of Chemistry, Graduate School of Advanced Science and Engineering, Hiroshima University, Higashi-Hiroshima 739-8526, Japan

ACKNOWLEDGMENT

We are grateful to Dr. Yuri Ito, Dr. Keiji Ohshima, and Prof. Fuminori Misaizu (Tohoku University) for fruitful discussions and Prof. Minoru Abe (Hiroshima University) for her expert advice on quantum chemical calculations. This work was financially supported by JSPS KAKENHI (Grant Numbers: JP19K15507 and JP22K14649), Futaba Foundation, and Electronic Technology Research Foundation of Chugoku. Calculations were performed at the Research Center for Computational Science, Okazaki, Japan.

REFERENCES

- (1) Müller-Dethlefs, K.; Hobza, P. Noncovalent Interactions: A Challenge for Experiment and Theory. *Chem. Rev.* **2000**, *100*, 143–167.
- (2) Felker, P. M.; Maxton, P. M.; Schaeffer, M. W. Nonlinear Raman Studies of Weakly Bound Complexes and Clusters in Molecular Beams. *Chem. Rev.* **1994**, *94*, 1787–1805.
- (3) Celi, F. G.; Janda, K. C. Vibrational Spectroscopy, Photochemistry, and Photophysics of Molecular Clusters. *Chem. Rev.* **1986**, *86*, 507–520.
- (4) Brutschy, B. The Structure of Microsolvated Benzene Derivatives and the Role of Aromatic Substituents. *Chem. Rev.* **2000**, *100*, 3891–3920.
- (5) Bieske, E. J.; Maier, J. P. Spectroscopic Studies of Ionic Complexes and Clusters. *Chem. Rev.* **1993**, *93*, 2603–2621.
- (6) Wang, D.; Fujii, A. Spectroscopic Observation of Two-Center Three-Electron Bonded (Hemi-Bonded) Structures of $(\text{H}_2\text{S})_n^+$ Clusters in the Gas Phase. *Chem. Sci.* **2017**, *8*, 2667–2670.
- (7) Kominato, M.; Fujii, A. Infrared Spectroscopy of $[\text{H}_2\text{O}-\text{X}_n]^+$ ($n = 1-3$, $\text{X} = \text{N}_2$, CO_2 , CO and N_2O) Radical Cation Clusters: Competition between Hydrogen Bond and Hemibond Formation of the Water Radical Cation. *Phys. Chem. Chem. Phys.* **2023**, *25*, 14726–14735.
- (8) Iguchi, A.; Singh, A.; Bergmeister, S.; Azhagesan, A. A.; Mizuse, K.; Fujii, A.; Tanuma, H.; Azuma, T.; Scheier, P.; Kuma, S.; et al. Isolation and Infrared Spectroscopic Characterization of Hemibonded Water Dimer Cation in Superfluid Helium Nanodroplets. *J. Phys. Chem. Lett.* **2023**, *14*, 8199–8204.
- (9) Hiraoka, K.; Fujimaki, S.; Aruga, K.; Yamabe, S. Frontier-Controlled Structures of the Gas-Phase $\text{A}^+(\text{CS}_2)_n$ Clusters, $\text{A}^+ = \text{S}_2^+$, CS_2^+ , S_2^- , and CS_2^- . *J. Phys. Chem.* **1994**, *98*, 1802–1809.
- (10) Inokuchi, Y.; Ebata, T. IR Photodissociation Spectroscopy of $(\text{OCS})_n^+$ and $(\text{OCS})_n^-$ Cluster Ions: Similarity and Dissimilarity in the Structure of CO_2 , OCS , and CS_2 Cluster Ions. *J. Chem. Phys.* **2015**, *142*, 214306.
- (11) Inokuchi, Y.; Matsushima, R.; Kobayashi, Y.; Ebata, T. Ion Core Structure in $(\text{N}_2\text{O})_n^+$ ($n = 2-8$) Studied by Infrared Photodissociation Spectroscopy. *J. Chem. Phys.* **2009**, *131*, 044325.
- (12) Hiberty, P. C.; Humbel, S.; Archirel, P. Nature of the Differential Electron Correlation in Three-Electron Bond Dissociations. Efficiency of a Simple Two-Configuration Valence Bond Method with Breathing Orbitals. *J. Phys. Chem.* **1994**, *98*, 11697–11704.
- (13) Chatterjee, K.; Matsumoto, Y.; Dopfer, O. Aromatic Charge Resonance Interaction Probed by Infrared Spectroscopy. *Angew. Chem., Int. Ed.* **2019**, *58*, 3351–3355.

- (14) Johnson, M. A.; Alexander, M. L.; Lineberger, W. C. Photodissociation Cross Sections for Mass-Selected Ion Clusters: $(\text{CO}_2)_n^+$. *Chem. Phys. Lett.* **1984**, *112*, 285–290.
- (15) Smith, G. P.; Lee, L. C. Photodissociation of Atmospheric Positive Ions. II. 3500–8600 Å. *J. Chem. Phys.* **1978**, *69*, 5393–5399.
- (16) Inokuchi, Y.; Nishi, N. Photodissociation Spectroscopy of Benzene Cluster Ions in Ultraviolet and Infrared Regions: Static and Dynamic Behavior of Positive Charge in Cluster Ions. *J. Chem. Phys.* **2001**, *114*, 7059–7065.
- (17) Ohashi, K.; Nishi, N. Photodissociation Spectroscopy on Charge Resonance Band of $(\text{C}_6\text{H}_6)_2^+$ and $(\text{C}_6\text{H}_6)_3^+$. *J. Phys. Chem.* **1992**, *96*, 2931–2932.
- (18) Ohashi, K.; Nakai, Y.; Shibata, T.; Nishi, N. Photodissociation Spectroscopy of $(\text{C}_6\text{H}_6)_2^+$. *Laser Chem.* **1994**, *14*, 3–14.
- (19) Pieniazek, P. A.; Krylov, A. I.; Bradforth, S. E. Electronic Structure of the Benzene Dimer Cation. *J. Chem. Phys.* **2007**, *127*, 044317.
- (20) Stephan, K.; Futrell, H.; Peterson, I.; Castleman, A. W.; Märk, T. D. An Electron Impact Study of Carbon Dioxide Dimers in a Supersonic Molecular Beam: Appearance Potentials of $(\text{CO}_2)_2^+$, $(\text{CO CO}_2)^+$, and $(\text{Ar CO}_2)^+$. *J. Chem. Phys.* **1982**, *77*, 2408–2415.
- (21) Futrell, J. H.; Stephan, K.; Märk, T. D. The Metastable and Collision-Induced Dissociation of Propane, CO_2 -Cluster, and NH_3 -Cluster Ions. *J. Chem. Phys.* **1982**, *76*, 5893–5901.
- (22) Ohashi, K.; Adachi, K.; Nishi, N. Unimolecular Dissociation Kinetics of Benzene Cluster Ions. *Bull. Chem. Soc. Jpn.* **1996**, *69*, 915–924.
- (23) Jiang, J. C.; Wang, Y. S.; Chang, H. C.; Lin, S. H.; Lee, Y. T.; Niedner-Schatteburg, G.; Chang, H. C. Infrared Spectra of $\text{H}^+(\text{H}_2\text{O})_{5-8}$ Clusters: Evidence for Symmetric Proton Hydration. *J. Am. Chem. Soc.* **2000**, *122*, 1398–1410.
- (24) Wu, C. C.; Lin, C. K.; Chang, H. C.; Jiang, J. C.; Kuo, J. L.; Klein, M. L. Protonated clathrate cages enclosing neutral water molecules: $\text{H}^+(\text{H}_2\text{O})_{21}$ and $\text{H}^+(\text{H}_2\text{O})_{28}$. *J. Chem. Phys.* **2005**, *122*, 074315.
- (25) Katada, M.; Hsu, P.-J.; Fujii, A.; Kuo, J.-L. Temperature and Size Dependence of Characteristic Hydrogen-Bonded Network Structures with Ion Core Switching in Protonated $(\text{Methanol})_{6-10}$ – $(\text{Water})_1$ Mixed Clusters: A Revisit. *J. Phys. Chem. A* **2017**, *121*, 5399–5413.
- (26) Ishikawa, H.; Kuru, L.; Yagi, R.; Kato, R.; Kasahara, Y. Quantitative Temperature Dependence of the Microscopic Hydration Structures Investigated by Ultraviolet Photodissociation Spectroscopy of Hydrated Phenol Cations. *J. Phys. Chem. Lett.* **2017**, *8*, 2541–2546.
- (27) Shimamori, T.; Kuo, J. -L.; Fujii, A. Stepwise Internal Energy Change of Protonated Methanol Clusters by Using the Inert Gas Tagging. *J. Phys. Chem. A* **2016**, *120*, 9203–9208.
- (28) Wang, Y. -S.; Tsai, C. -H.; Lee, Y. T.; Chang, H. -C.; Jiang, J. C.; Asvany, O.; Schlemmer, S.; Gerlich, D. Investigations of Protonated and Deprotonated Water Clusters Using a Low-Temperature 22-Pole Ion Trap. *J. Phys. Chem. A* **2003**, *107*, 4217–4225.
- (29) Buck, U.; Huisken, F. Infrared Spectroscopy of Size-Selected Water and Methanol Clusters. *Chem. Rev.* **2000**, *100*, 3863–3890.
- (30) Gadre, S. R.; Yeole, S. D.; Sahu, N. Quantum Chemical Investigations on Molecular Clusters. *Chem. Rev.* **2014**, *114*, 12132–12173.
- (31) Gardenier, G. H.; Johnson, M. A.; McCoy, A. B. Spectroscopic Study of the Ion–Radical H-Bond in H_4O_2^+ . *J. Phys. Chem. A* **2009**, *113*, 4772–4779.
- (32) Inokuchi, Y.; Soga, K.; Hirai, K.; Kida, M.; Morishima, F.; Ebata, T. Ultraviolet Photodissociation Spectroscopy of the Cold $\text{K}^+\text{-Calix[4]arene}$ Complex in the Gas Phase. *J. Phys. Chem. A* **2015**, *119*, 8512–8518.
- (33) Boyarkin, O. V.; Mercier, S. R.; Kamariotis, A.; Rizzo, T. R. Electronic Spectroscopy of Cold, Protonated Tryptophan and Tyrosine. *J. Am. Chem. Soc.* **2006**, *128*, 2816–2817.
- (34) Fujihara, A.; Matsumoto, H.; Shibata, Y.; Ishikawa, H.; Fuke, K. Photodissociation and Spectroscopic Study of Cold Protonated Dipeptides. *J. Phys. Chem. A* **2008**, *112*, 1457–1463.
- (35) Goebbert, D. J.; Garand, E.; Wende, T.; Bergmann, R.; Meijer, G.; Asmis, K. R.; Neumark, D. M. Infrared Spectroscopy of the Microhydrated Nitrate Ions $\text{NO}_3^-(\text{H}_2\text{O})_{1-6}$. *J. Phys. Chem. A* **2009**, *113*, 7584–7592.
- (36) Inokuchi, Y.; Boyarkin, O. V.; Kusaka, R.; Haino, T.; Ebata, T.; Rizzo, T. R. UV and IR Spectroscopic Studies of Cold Alkali Metal Ion–Crown Ether Complexes in the Gas Phase. *J. Am. Chem. Soc.* **2011**, *133*, 12256–12263.
- (37) Kamrath, M. Z.; Garand, E.; Jordan, P. A.; Leavitt, C. M.; Wolk, A. B.; Van Stipdonk, M. J.; Miller, S. J.; Johnson, M. A. Vibrational Characterization of Simple Peptides Using Cryogenic Infrared Photodissociation of H_2 -Tagged, Mass-Selected Ions. *J. Am. Chem. Soc.* **2011**, *133*, 6440–6448.
- (38) Liu, H.-T.; Ning, C.-G.; Huang, D.-L.; Dau, P.-D.; Wang, L.-S. Observation of Mode-Specific Vibrational Autodetachment from Dipole-Bound States of Cold Anions. *Angew. Chem.* **2013**, *125*, 9146–9149.
- (39) Berdakin, M.; Féraud, G.; Dedonder-Lardeux, C.; Jouvet, C.; Pino, G. A. Excited States of Protonated DNA/RNA Bases. *Phys. Chem. Chem. Phys.* **2014**, *16*, 10643–10650.
- (40) Sekiguchi, T.; Tamura, M.; Oba, H.; Çarçarbal, P.; Lozada-Garcia, R. R.; Zehnacker-Rentien, A.; Grégoire, G.; Ishiuchi, S.; Fujii, M. Molecular Recognition by a Short Partial Peptide of the Adrenergic Receptor: A Bottom-Up Approach. *Angew. Chem. Int. Ed.* **2018**, *57*, 5626–5629.
- (41) Muramatsu, S.; Tokizane, T.; Inokuchi, Y. One-Dimensionally Conjugated Carbocyanine Dyes Isolated under Cold Gas-Phase Conditions: Electronic Spectra and Photochemistry. *J. Phys. Chem. A* **2022**, *126*, 8127–8135.
- (42) Muramatsu, S.; Ohshimo, K.; Shi, Y.; Kida, M.; Shang, R.; Yamamoto, Y.; Misaizu, F.; Inokuchi, Y. Gas-Phase Characterization of Hypervalent Carbon Compounds Bearing 7-6-7-Ring Skeleton: Penta- versus Tetra-Coordinate Isomers. *Chem. Eur. J.* **2023**, *29*, e202203163.
- (43) Zhou, M.; Andrews, L. Infrared Spectra of the CS_2^- , CS_2^+ , and C_2S_4^+ Molecular Ions in Solid Neon and Argon. *J. Chem. Phys.* **2000**, *112*, 6576–6582.
- (44) Kobayashi, Y.; Inokuchi, Y.; Ebata, T. Ion Core Structure in $(\text{CS}_2)_n^+$ and $(\text{CS}_2)_n^-$ ($n = 3-10$) Studied by Infrared Photodissociation Spectroscopy. *J. Chem. Phys.* **2008**, *128*, 164319.
- (45) Illies, A. J.; McKee, M. L.; Schlegel, H. B. Ab Initio Study of the CO_2 Dimer and the CO_2 Ion Complexes $(\text{CO}_2)_2^+$ and $(\text{CO}_2)_3^+$. *J. Phys. Chem.* **1987**, *91*, 3489–3494.
- (46) Nakashima, Y.; Okutsu, K.; Fujimoto, K.; Ito, Y.; Kanno, M.; Nakano, M.; Ohshimo, K.; Kono, H.; Misaizu, F. Visible Photodissociation of the CO_2 Dimer Cation: Fast and Slow Dissociation Dynamics in the Excited State. *Phys. Chem. Chem. Phys.* **2019**, *21*, 3083–3091.
- (47) Inokuchi, Y.; Muraoka, A.; Nagata, T.; Ebata, T. An IR Study of $(\text{CO}_2)_n^+$ ($n = 3-8$) Cluster Ions in the 1000–3800 cm^{-1} Region. *J. Chem. Phys.* **2008**, *129*, 044308.
- (48) Zhou, M.; Andrews, L. Infrared Spectra of the C_2O_4^+ Cation and C_2O_4^- Anion Isolated in Solid Neon. *J. Chem. Phys.* **1999**, *110*, 6820–6826.
- (49) Shkrob, I. A. Ionic Species in Pulse Radiolysis of Supercritical Carbon Dioxide. 2. Ab Initio Studies on the Structure and Optical Properties of $(\text{CO}_2)_n^+$, $(\text{CO}_2)_2^-$, and CO_3^- Ions. *J. Phys. Chem.* **2002**, *106*, 11871–11881.
- (50) McKee, M. L. A Theoretical Study of $(\text{N}_2\text{O})_2^+$, $(\text{CO}_2)_2^+$ and $\text{N}_2\text{O}^+\text{-CO}_2$. Comparison of the Two-Center-Three-Electron Bond and the Ion-Dipole Complex. *Chem. Phys. Lett.* **1990**, *165*, 265–271.
- (51) Kanno, M.; Maeda, T.; Nakashima, Y.; Misaizu, F.; Kono, H. A Fast and Robust Trajectory Surface Hopping Method: Application to

the Intermolecular Photodissociation of a Carbon Dioxide Dimer Cation $(\text{CO}_2)_2^+$. *J. Chem. Phys.* **2021**, *154*, 164108.

(52) Ishiuchi, S.; Wako, H.; Kato, D.; Fujii, M. High-Cooling-Efficiency Cryogenic Quadrupole Ion Trap and UV-UV Hole Burning Spectroscopy of Protonated Tyrosine. *J. Mol. Spectrosc.* **2017**, *332*, 45–51.

(53) Kang, H.; Féraud, G.; Lardeux, C. D.; Jouvét, C. New Method for Double-Resonance Spectroscopy in a Cold Quadrupole Ion Trap and Its Application to UV–UV Hole-Burning Spectroscopy of Protonated Adenine Dimer. *J. Phys. Chem. Lett.* **2014**, *5*, 2760–2764.

(54) Pino, G. A.; Jara-Toro, R. A.; Aranguren-Abrate, J. P.; Dedonder-Lardeux, C.; Jouvét, C. Dissociative Photodetachment vs. Photodissociation of Aromatic Carboxylates: The Benzoate and Naphthoate anions. *Phys. Chem. Chem. Phys.* **2019**, *21*, 1797–1804.

(55) MacAleese, L.; Maitre, P. Infrared Spectroscopy of Organometallic Ions in the Gas Phase: From Model to Real World Complexes. *Mass Spectrom. Rev.* **2007**, *26*, 583–605.

(56) Frisch, M. J.; Trucks, G. W.; Schlegel, H. B.; Scuseria, G. E.; Robb, M. A.; Cheeseman, J. R.; Scalmani, G.; Barone, V.; Petersson, G. A.; Nakatsuji, H.; et al. *Gaussian 16, Revision C.02*; Gaussian, Inc.: Wallingford, CT, 2019.

(57) Inokuchi, Y.; Kobayashi, Y.; Muraoka, A.; Nagata, T.; Ebata, T. Structures of Water- CO_2 and Methanol- CO_2 Cluster ions: $[\text{H}_2\text{O} \cdot (\text{CO}_2)_n]^+$ and $[\text{CH}_3\text{OH} \cdot (\text{CO}_2)_n]^+$ ($n = 1-7$). *J. Chem. Phys.* **2009**, *130*, 154304.

(58) Rumble, J. R. *CRC Handbook of Chemistry and Physics*, 103rd ed.; CRC Press, Boca Raton, 2022.

(59) Note that this energy value is just a difference in total electronic energies without contributions from vibrational zero-point corrections and entropy factors. In this sense, this relative population value is just a qualitative estimation; however, the main discussion (drastic difference between ambient and cryogenic temperatures) remains valid.